



ELSEVIER

Coastal Engineering 41 (2000) 41–62

**COASTAL
ENGINEERING**

www.elsevier.com/locate/coastaleng

The spectral wave model, WAM, adapted for applications with high spatial resolution

Jaak Monbaliu^{a,*}, Roberto Padilla-Hernández^a,
Julia C. Hargreaves^b, Juan Carlos Carretero Albiach^c,
Weimin Luo^{b,1}, Mauro Sclavo^{b,2}, Heinz Günther^d

^a *Hydraulics Laboratory, Katholieke Universiteit Leuven, de Croylaan 2, Heverlee B-3001, Belgium*

^b *Proudman Oceanographic Laboratory, Bidston Observatory, Birkenhead CH43 7RA, UK*

^c *Programa de Clima Marítimo (Ente Público Puertos del Estado), Antonio López 81, Madrid E-28026, Spain*

^d *Institute of Hydrophysics, GKSS Research Centre, Max-Planck Str., Geesthacht D-21502, Germany*

Abstract

New features have been added and several necessary changes have been made to the standard WAM-cycle4 (WAMC4) model code for it to run efficiently when applied to shallow water regions. The restriction of having a source term integration time step smaller than or equal to the propagation time step was relaxed, considerably reducing the computational time needed. An additional reduction in computing time and an increase in accuracy were obtained by introducing a split-frequency time step. There is now a choice of using the octant or quadrant coordinate system for the propagation of the wave energy. The source term integration and, more particularly, the use of a limiter on the energy growth, were studied. For the evaluation of the energy decay in shallow water areas, different bottom friction formulations and an expression for the energy dissipation due to depth-induced wave breaking were added to the code. The procedure to make nested runs was changed in order to save data storage space and time spent on input/output (I/O) operations. Several other changes were done in order to improve the accuracy in high-resolution applications. A number of simple or idealised example applications are included to illustrate some of these enhancements. © 2000 Elsevier Science B.V. All rights reserved.

Keywords: Coast; Pre-operational modelling; Shallow water; WAM; Wave modelling; Wave spectra

* Corresponding author. Fax: +32-16-321989.

E-mail address: jaak.monbaliu@bwk.kuleuven.ac.be (J. Monbaliu).

¹ Previously at KU Leuven, Belgium. Present address: Environment Canada, Toronto, Canada.

² Present address: ISDGM, Palazzo Papadopoli, San Polo 1364, Venezia I-30125, Italy.

1. Introduction

The development of a high-resolution spectral wave model capable of dealing with shallow water conditions and incorporating the interaction due to tide and surge was an important aspect of the EU MAST III project, PROMISE (Pre-Operational Modelling In the Seas of Europe)(also see Prandle, 2000). Waves form an integral part of the envisaged pre-operational framework of mathematical modelling tools that were thought to be necessary to quantify the rates and scales of the sediment exchange between the coast and the nearshore zone. At the beginning of the project, the option of improving the capabilities of the WAM-cycle4 (WAMC4) model (Günther et al., 1992) was decided upon.

Three objectives were planned for the PROMISE wave modelling effort, the second of which is discussed in detail in this paper.

The first objective was an intercomparison exercise on the North Sea scale for a 1-month period. The main purpose of this exercise was to align the efforts of the participating institutions. Details of this intercomparison exercise can be found in Monbaliu et al. (1997, 1999). Although this could not be considered as an exhaustive test, the different model implementations provided similar results and the agreement with buoy and satellite measurements was acceptable and comparable to other values published in the literature.

The second objective was the use of a spectral wave model for applications in coastal areas, i.e. shallow water areas where high-spatial resolution (order of 1 km) is needed. However, the standard WAMC4 code presented a number of limitations. The coding developments made for these coastal scale applications will be described in more detail in this paper, with particular emphasis on computer central processing unit (CPU) efficiency and improved input/output (I/O). Some developments are illustrated with simple or idealised example applications. A practical example of the use of this enhanced model can be found in Prandle et al. (2000).

The third objective was the coupling of the spectral wave model with a surge model in order to incorporate their mutual interaction in the output of the hydrodynamic field parameters. In coastal areas, the effects of tides and currents on waves can be considerable. A detailed description of the interaction process, the consequences and a sensitivity analysis can be found in Ozer et al. (2000).

2. Wave modelling

2.1. Phase-resolving vs. phase-averaged models

Battjes (1994) considers two families of shallow water wave models. They are phase-resolving (for rapidly varying waves, i.e. waves that have phase-averaged local properties which vary rapidly within distances of the order of one wavelength) and phase-averaged models (for slowly varying waves). In most cases, the assumption of phase randomness is a good approximation for the description of wind-generated waves. It is known that the spectral wave energy distribution contains sufficient information to

determine the most important parameters of the wave field. The exact location of the sea surface is not known in the strict sense but it is known in a statistical sense. If at all possible, it is most economical to compute the energy spectrum (a phase-averaged quantity) with a phase-averaged model. Phase-resolving models describe the sea surface as a function of time but are computationally very demanding and should be used only when strictly required. Only the mathematical description of strong diffraction and possibly of triad interaction requires phase-resolving models like gentle slope equation or Boussinesq models.

The wave modelling effort in the PROMISE project envisaged different applications. In terms of spatial scale, they ranged from large-scale applications such as the North Sea where a resolution of the order of 20–50 km seemed adequate, to small-scale applications such as the Holderness area where a spatial resolution in the order of 1 km is needed. None of the applications had to deal with rapid variations. A phase-averaged model was therefore the logical choice for the PROMISE project. It contains the necessary physics to describe the spectrum adequately, covers the space and time scales needed, and is reasonable in terms of computational overheads. The model, WAMC4 (Günther et al., 1992), was chosen because it was, at the start of the project, the only state-of-the-art model readily available in the public domain. The WAMC4 model is used, e.g., for global operational wave forecasting at the European Centre for Medium-Range Weather Forecasts (ECMWF), and regionally in many other meteorological centres around the world. In deep and intermediate water, wave hindcasts are fairly reliable and efficient. There was also considerable experience and familiarity with this model at a number of the institutes participating in PROMISE.

During the time that the PROMISE project was underway, other researchers had devoted much effort to developing the SWAN (Simulating Waves Nearshore) model. This model is now also in the public domain (see, e.g., Ris, 1997; Ris et al., 1999; Booij et al., 1999). SWAN is very similar to WAM, but was conceived as a shallow water model. It uses an implicit scheme for wave propagation and includes relevant shallow water source terms such as depth-induced breaking and triad wave–wave interactions. Also worth mentioning is the development of the so-called K-model (Günther and Rosenthal, 1997; Schneggenburger, 1998). It is a phase-averaged model specially designed for application to coastal tidal environments. A new feature of the model is the consideration of wave dissipation by interaction with turbulence. The dynamics is formulated to allow for a convenient treatment of non-stationary water level and current fields. As part of the PROMISE project, the K-model was validated and applied for investigations in the Sylt–Rømø tidal basin (Schneggenburger et al., 2000).

2.2. The standard WAMC4 model

WAMC4 is a third-generation wave model, which solves the wave transport equation explicitly without any a priori assumptions on the shape of the wave energy spectrum.

The equation solved in the code reads in Cartesian coordinates as:

$$\frac{\partial F}{\partial t} + \frac{\partial}{\partial x}(c_x F) + \frac{\partial}{\partial y}(c_y F) + \sigma \frac{\partial}{\partial \sigma} \left(c_\sigma \frac{F}{\sigma} \right) + \frac{\partial}{\partial \theta} (c_\theta F) = S_{\text{tot}}, \quad (1)$$

where $F(t, x, y, \sigma, \theta)$ is the wave energy spectrum, t is the time, σ is the intrinsic angular frequency, θ is the wave direction measured clockwise from the true north, c_x and c_y are the propagation velocities in geographical space, and c_σ and c_θ are the propagation velocities in spectral space (frequency and directional space). The left-hand side of the above equation represents the local rate of change of wave energy density, propagation in geographical space, and shifting of frequency and refraction due to the spatial variation of the depth and current. The right-hand side represents all effects of generation and dissipation of the waves including wind input S_{in} , white capping dissipation S_{ds} , non-linear quadruplet wave–wave interactions S_{nl} and bottom friction dissipation S_{bf} . A detailed description of the WAMC4 model can be found in Günther et al. (1992) and Komen et al. (1994). One can show that Eq. 1 is equivalent to the action density conservation equation. This is important in the presence of currents since in that case, wave action and not wave energy is conserved (for a more detailed explanation, see also Ozer et al., 2000).

WAMC4 is also a state-of-the-art third-generation spectral wave model specifically designed for global and shelf sea applications. It can run in deep or shallow water and includes depth and current refraction (steady depth and current field only). It can be set up for any local or global grid with a prescribed data set, and grids may be nested for fine scale applications.

Computationally, Eq. 1 is solved in two parts. The propagation of the energy density is solved by discretisation of the left-hand side, setting the right-hand side equal to zero, into a first-order explicit upwind scheme. The time step for this part is limited by the Courant–Friedrichs–Lewy (CFL) stability condition, and may be calculated on either a spherical or Cartesian grid. The source term contribution is then added using a semi-implicit forward time scheme.

2.3. Difficulties in using WAMC4 in high-resolution applications

Some enhancements were required before the standard WAMC4 model could be applied to coastal areas. The obstacles encountered may be placed in the following categories: propagation scheme, source terms, CPU demand, I/O and other.

One of the main restrictions in the standard WAMC4 code was the fact that the source integration time step had to be shorter than or equal to the propagation time step. Keeping the number of bins in the frequency domain constant, the computational cost of the model grows as $m \times n^3$ when the wave directional resolution increases m times and the space resolution increases n times, because the propagation time step is limited by the CFL criterion. Consequently, operational use of WAMC4 in coastal regions is computationally very expensive, with 1 km resolution applications running at the order of real time on current workstations.

A second propagation problem was encountered for waves moving nearly parallel and close to the coast. There is an unrealistic loss of energy at the boundary points caused by the large second-order diffusion error of the first-order upwind scheme. The ‘numerical’ losses tend to spread rapidly through the geographical and spectral domain.

WAMC4 only takes into account stationary current fields and water depths. The shallow coastal zone is a dynamic region where changing currents and depths due to tide

and surge play an important role in modifying the wave field. In this region, current field and water depths are at least slowly varying and must, therefore, be incorporated into the model in order to predict such quantities as shelf sediment transport.

Additional source terms were considered necessary to deal with the shallow water physics. The bottom friction dissipation term in WAMC4 is modelled by the empirical JONSWAP expression. This formulation does not contain information about the processes in the wave boundary layer and it is therefore difficult to extract bottom stresses. This is especially true in a combined wave–current field. Moreover, in extreme shallow water (surf zone), the process of depth-induced wave breaking becomes dominant over all other processes. Also, triad wave–wave interactions might become important. These last two processes are not included as source terms in WAMC4.

A coastal application will typically use a fine grid nested into a coarser grid. WAMC4 writes the boundary conditions for the finer grid to disk every propagation time step. Before the fine grid run, these boundary conditions need to be interpolated in space and time to the time and space scales of the fine grid. In addition to being time-consuming in terms of I/O, this procedure devours tremendous amounts of disk space.

Some other items, mostly programming details, needed to be solved as well. The WAMC4 model limits all time steps to be an integer multiple of 1 min. This strongly constrains applications of the model at high resolutions. If space resolution is better than 1.13 km and the minimum frequency is set at 0.04177 Hz (standard value), the propagation time step must be smaller than 1 min. In shallow water applications, the grid resolution can become a fraction of a degree. Problems arise when resolutions, given in degrees in the original WAMC4 code, are fractional numbers. In such cases, the accuracy for the locations of the computational grid points might be insufficient and the number of computational points computed by the program might not correspond with the number of points given by the user. Also, the accuracy in the locations of the I/O points can be insufficient so that the difference in location for an output point computed by WAMC4 and then introduced by the user in the post-processing modules of WAMC4 can become so large (relatively) that no model information is found.

In local applications where it can be justified to keep the boundary conditions constant, steady state conditions can be reached. Continuing the run can lead to unnecessary use of the computational resources.

3. WAMC4-P for fine-scale coastal applications

3.1. Introduction

The obstacles encountered while running WAMC4 in high-resolution applications were identified in Section 2.3. Modifications made to the code are described below, and the effects are illustrated with a number of examples compiled from various tests carried out in the North Sea or coastal scales. The areas of the model implementations are

described in Section 3.2 below. The illustrative examples and the discussion and interpretation of the results follow immediately after the theoretical background. Special attention is paid to the aspects of speed-up and improved I/O without compromising on output quality. In the remainder of the text, we will refer to the PROMISE version of WAMC4 as WAMC4-P. The changes in the code required to obtain WAMC4-P from the standard WAMC4 code have been documented in a technical report [(Monbaliu et al., 1998)].

3.2. Model implementations

3.2.1. The Holderness area

The WAMC4-P code was implemented on a 2.4-km resolution grid of the Holderness area. Holderness is situated on the east coast of England. The bathymetry and the output locations are given in Fig. 1. For more details about this region, the reader is referred to Prandle et al. (2000). The wave spectra were modelled with 25 frequency and 12 directional bands. The directional resolution was therefore equal to 30°. The frequency bands were set to a logarithmic scale, with $\Delta f/f = 0.1$. The lowest and highest frequencies are 0.04177 and 0.4114 Hz, respectively.

3.2.2. The North Sea area

For the North Sea area test, two different implementations were used. The first is a three-level nested grid implementation using spherical coordinates. To account for swell

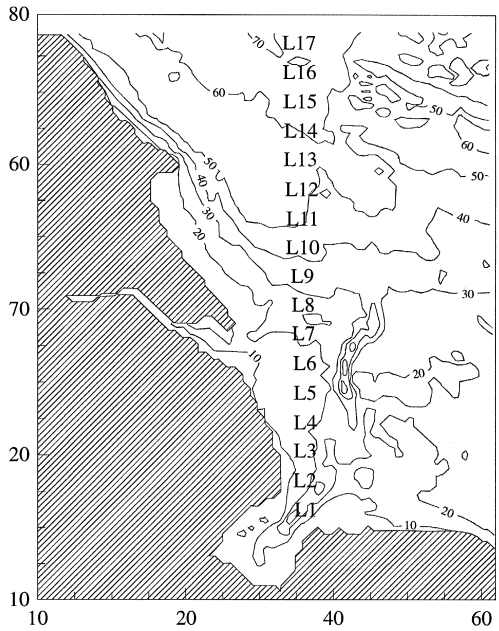


Fig. 1. The Holderness area. L1 to L17 are locations for model output.

generated in the Norwegian Sea, the coarse grid covers the area 48°N–70°N, 7°W–12°E and this has a resolution of 1/3° latitude and 2/3° longitude. The intermediate grid covers 50°N–52°N, 0°W–4°E with a resolution of 1/24° latitude and 1/12° longitude. The fine grid covers the area 51°N–51.5°N, 2.5°E–3.6°E with a resolution of 1/96° in both latitude and longitude, corresponding to a grid size of about 1.2 km. The second is a two-level nested grid implementation (resolution of 50 × 50 km² for the coarse and 10 × 10 km² for the nested grid), which covers basically the same area as the coarse grid and intermediate spherical grid. A stereographic projection was applied to enable the use of Cartesian coordinates. The directional and frequency grids were identical to the Holderness implementation.

3.3. Code modification

3.3.1. Propagation

3.3.1.1. Improved stability for large depth gradients. The first-order advection algorithm becomes unstable when large depth gradients are present. Advection is multi-dimensional in the same time step. In particular, for high-resolution applications of the model in shallow water, the advection time step frequently needs to be reduced for a few grid points where high gradients in the bathymetry are found. For a specific energy component of the spectrum F_j at time step $n + 1$, the first-order explicit advection equation, after being rearranged, takes the form:

$$F_j^{n+1} = (1 - \alpha_1 - \alpha_2 - \dots - \alpha_n)F_j^n + \alpha'_1 F_1^n + \alpha'_2 F_2^n + \dots + \alpha'_n F_n^n, \quad (2)$$

where α_i and α'_i refer to the appropriate coefficients in the upwind numerical scheme and $F_1^n, F_2^n \dots F_n^n$ refer to the upwind components of the energy advection (from different spectra but from the same frequency direction bin for latitude and longitude advection, and from the same spectrum but from a different direction–frequency bin for propagation in direction and frequency). The number of terms, N , depends on the specifications supplied by the user (deep or shallow water run, depth refraction and/or current refraction included). This can be represented by a straight line of slope $(1 - S)$ and intercept B :

$$F_j^{n+1} = (1 - S)F_j^n + B. \quad (3)$$

Making $\alpha_1, \alpha_2, \dots, \alpha_n < 1$ does not assure stability. The value of $S (= \alpha_1 + \alpha_2 + \dots + \alpha_n)$ also needs to be checked: if $(0 < S \leq 1)$ then stable, if $(1 < S \leq 2)$ then probably unstable. Fig. 2 shows how the slope changes with the value of S and how negative and non-convergent values can be obtained, making the advection algorithm unstable. A new subroutine called in the initialisation phase of the wave model checks the stability for all grid points and directions at the lowest frequency. The run is stopped if $\alpha > 1$ or $S > 2$. If S is between 1 and 2, the required time step for the grid point is computed and given in the output as user information.

3.3.1.2. Altering the source integration and propagation time steps. The contributions from the propagation terms and from the source terms are calculated separately. For a

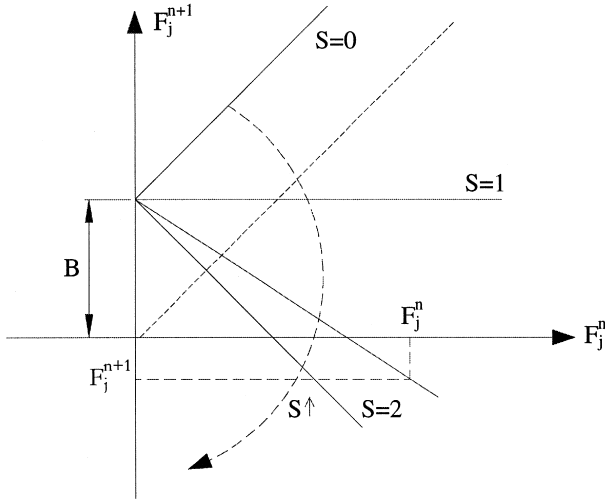


Fig. 2. First-order upwind advection algorithm. For $S > 1$, negative energy can be produced and the system can become unstable.

typical WAMC4 application, 75% of the CPU time is needed for the calculation of the source terms, 20% for the I/O operations and only about 5% for the propagation calculation. The CFL condition limits the maximum time step to be used in the propagation scheme. Clearly, the efficiency of the source term calculation is critical for decreasing model run time so that fine resolution implementations become feasible.

The source terms are calculated as point processes, meaning that they only use spectral information from one location in space. The time scale of the physical processes associated with the source terms does not necessarily scale with grid resolution in the same way as the CFL condition imposes time step restrictions on the propagation. There is, therefore, no reason why, in fine resolution applications, the source term time step should not be greater than the propagation time step. The code has been modified to allow an integer number of propagation time steps to be performed for each source term time step.

The discretised version of Eq. 1 expresses the spectrum F^{n+1} at the level t^{n+1} ($= t^n + \Delta t$; Δt is the source term time step) in terms of F^n . Eq. 1 is first solved without source terms (i.e. the right-hand side of Eq. 1 is zero). Assume that one source term time step is split into m (an integer ≥ 1) propagation time steps. The increment in wave energy spectrum due to propagation at time level $t^{n+r/m}$ ($0 \leq r \leq m - 1$) is expressed as:

$$\begin{aligned} \Delta_{\text{prop}} F^{n+\frac{r}{m}} &= \left(F^{n+\frac{r+1}{m}} - F^{n+\frac{r}{m}} \right)_{\text{prop}} \\ &= - \left[\frac{\partial}{\partial x} (c_x F) + \frac{\partial}{\partial y} (c_y F) + \sigma \frac{\partial}{\partial \sigma} \left(c_\sigma \frac{F}{\sigma} \right) + \frac{\partial}{\partial \theta} (c_\theta F) \right] \Delta t_p^{\text{max}}. \end{aligned} \tag{4}$$

The equation is evaluated using a split first-order upwind scheme. Here, m equals the ratio of the source term time step Δt_{int} to the propagation time step $\Delta t_{\text{p}}^{\text{max}}$ at the highest frequency. Every $\Delta t_{\text{p}}^{\text{max}}$ can be split into several sub-propagation time steps, depending on frequency. After m propagation time steps (i.e. one source term time step), time level t^{n+1} is reached and the wave energy spectrum increment due to propagation thus becomes:

$$(F^{n+1} - F^n)_{\text{prop}} = \sum_{i=0}^{m-1} \Delta_{\text{prop}} F^{n+\frac{i}{m}} \tag{5}$$

Second, the source terms are integrated. Finally, the full spectrum at time level t^{n+1} is obtained by adding the propagation and source term contributions together.

Care should be taken in the use of this feature. In high growth situations, the time scale of variation of the non-linear interactions is small. Also in shallow water regions, the source term time step should not be so large that there is significant variation in the water depth between successive source term calculations.

With a source term time step that can become larger than the propagation time step, the proportion of the total CPU time used in calculating the propagation is, of course, increased. A further increase in the computational speed can be obtained by altering the propagation time step to be a function of frequency. Higher frequencies have a smaller group velocity. A longer time step can be used for slower propagating wave components, while retaining numerical stability. Therefore, a split-frequency time step numerical scheme was developed for wave propagation, which allows the propagation time step to be frequency-dependent.

Users only need to specify one propagation time step corresponding to any frequency other than the first one. The model will determine how many different propagation time steps are to be used according to the CFL conditions corresponding to different frequencies. In any case, the propagation time steps at different frequencies must be an integer multiple. The ratio of source term time step to propagation time steps must be an integer number (only possible in the present scheme) or the inverse of an integer number (as in the original scheme).

The modifications described in this subsection are illustrated with a simple example using the Holderness area set-up (see Section 3.2.1). Four tests, numbered H1–H4, were carried out with different propagation and source term time step combinations (see Table 1). A uniform southerly wind of 18.45 m s^{-1} was used. Note that the time step used in

Table 1
Four tests with different time steps for the case of a uniform wind blowing offshore of the Holderness region

	Propagation time step (s)	Source term time step (s)
H1	60 for all frequencies	60
H2	60 for the first frequency 120 for the remaining frequencies	360
H3	Idem H2	720
H4	Idem H2	1080

H1 is limited by the original scheme of the WAMC4 model. The limiter used was that of Eq. 13 from Luo and Sclavo (1997) (see Section 3.3.2.1).

Fig. 3 shows the growth of the significant wave height as a function of fetch for the four test runs along the fetch line L1–L17 (see Fig. 1) after 48 h. One can see that nearly identical growth curves are obtained for runs H1, H2 and H3. For the run H4 with a source term time step of 1080 s, the difference with the original scheme is about 5% for significant wave height and 1% for the mean frequency (plot not shown).

Fig. 4 shows the significant wave height as a function of time for the four test cases at locations L5 and L17. Similar growth curves (not shown) were found at other locations. The waves are fully developed in a few hours. The growth curves of the runs H1, H2 and H3 are very close. The significant wave height difference between the H1 and the H4 run is of the order of 5%. The mean frequency difference between the H1 and the H4 run is less than 2%. Some oscillations (numerical noise) are visible for the run H4, but these are not amplified with time. The corresponding one-dimensional frequency spectra are shown in Fig. 5 for runs H1 and H3. An overshoot is visible in the results of both runs and the energy difference at the peak frequency is less than 5%.

One of the crucial objectives to be achieved in the study was the improvement in the computational efficiency. Fig. 6 shows the relative CPU time used for the original propagation and source term integration scheme and the present scheme with different time steps combinations. Run H1 corresponds to the original scheme and limits the source term time step to be less than or equal to the propagation time step, set here to 60 s to ensure numerical stability. It is clear that the longer the source term integration time step, the more efficient the computation. Runs H3 and H4 illustrate that relaxing the constraint on the source term integration time step makes the computations nearly one

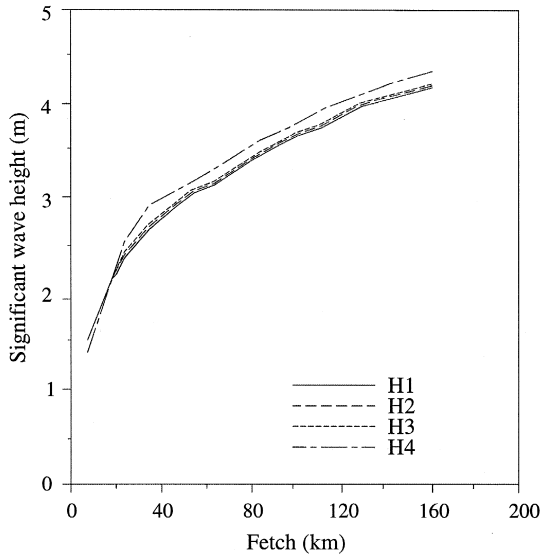


Fig. 3. Significant wave height as a function of fetch for uniform offshore wind. Test cases are given in Table 1.

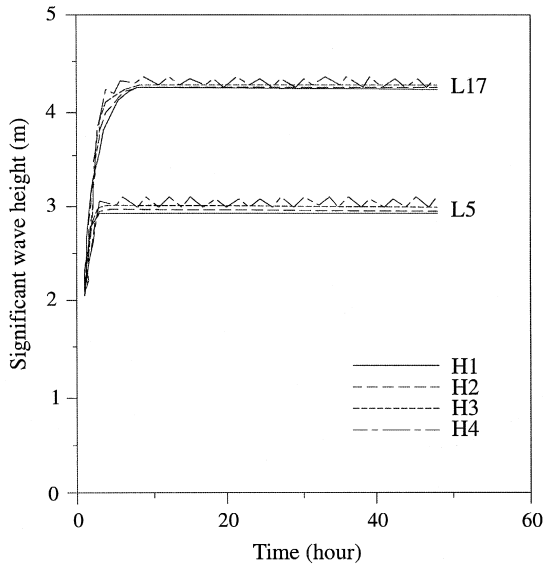


Fig. 4. Time series of significant wave height at locations L5 and L17 for the four test cases described in Table 1.

order of magnitude more efficient. However, for runs with a source term time step longer than that in run H4, the drastic reduction in CPU time will disappear. The relative contribution of the source term integration to the total computational time is no longer

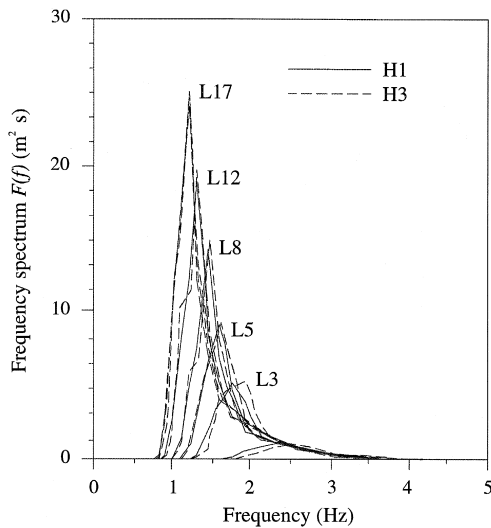


Fig. 5. Comparison of the one-dimensional frequency spectrum for different time steps. The test cases are given in Table 1 (run H1, $\Delta t_{prop} = \Delta t_{int} = 60$ s; run H3, $\Delta t_{prop} = 120$ s, $\Delta t_{int} = 720$ s).

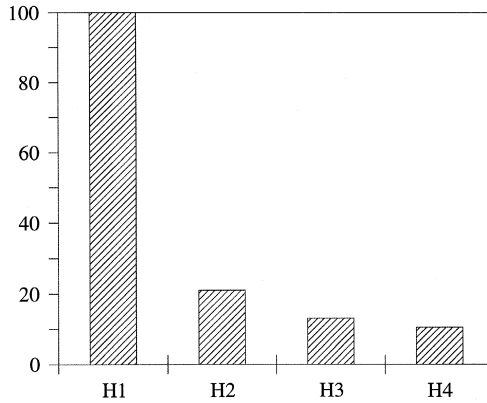


Fig. 6. The relative CPU time (%) for different time step combinations. The test cases are given in Table 1.

dominant when the source time step exceeds a certain number of times the propagation time step. The law of diminishing returns applies. Moreover, the results from run H4 with a source term time step of 1080 s already start to deviate from the ‘true’ H1 run results, which is not the case for the results of the H2 and H3 runs. This suggests that it remains wise to limit the source term time step to less than 20 min, in accordance to what is needed from a physical point of view. This accords with the suggestion in the WAMC4 manual of 600 s as a maximum time step for shallow water applications. Generally, the physical conditions (wind, currents, depth, etc.) do not change more rapidly and one can obtain a good compromise between accurate results and computational efficiency. Other experiments (not shown here) confirmed the above findings of nearly identical wave prediction results as long as the source term integration time step does not exceed 10–20 min.

3.3.1.3. An octant vs. a quadrant propagation scheme. In order to reduce the physically unrealistic energy loss at the boundary points in conditions such as when the waves are propagating parallel and close to the coast, an alternative propagation coordinate system was introduced into the WAMC4-P model. The characteristics and the mathematical details of the octant scheme can be found in Cavaleri and Sclavo (1998). Geometrical interpretations of the octant (new) and the quadrant coordinate system (standard in WAMC4) are given in Fig. 7. In the case of the octant advection scheme, eight possible propagation directions are defined (instead of four for the quadrant scheme), the four cardinal directions plus the four diagonals, splitting the advection space into eight parts. The energy at point A at time t^n is advected to the point P after one propagation time step. The vector AP is split into its two components AP_1 and AP_2 along the two axes AD and AC (see Fig. 7a), and the energy is considered to be advected as a whole to both P_1 and P_2 .

Then, the redistribution of energy is:

$$E_C^{n+1} = E_A^n \frac{AP_1}{AC}; \quad E_D^{n+1} = E_A^n \frac{AP_2}{AD}; \quad E_A^{n+1} = E_A^n - E_C^{n+1} - E_D^{n+1}. \quad (6)$$

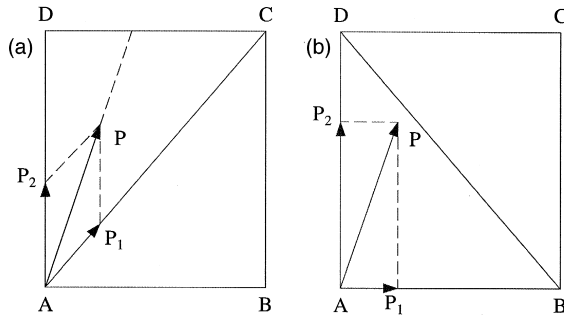


Fig. 7. Geometrical interpretation of the two schemes for first-order advection. The region AP_1PP_2 is influenced by one advection step. (a) Octant scheme, (b) quadrant scheme.

The distribution of energy in the quadrant propagation scheme is along the axes AB and AD (see Fig. 7b) and is therefore:

$$E_B^{n+1} = E_A^n \frac{AP_1}{AB} ; \quad E_D^{n+1} = E_A^n \frac{AP_2}{AD} ; \quad E_A^{n+1} = E_A^n - E_B^{n+1} - E_D^{n+1}. \quad (7)$$

One can see immediately that the energy lost (equal to that removed) at the land point D in the case of octant scheme is less than in the quadrant scheme (the vector AP_2 in Fig. 7a is smaller than the corresponding one in Fig. 7b).

As an illustrative example, hindcast runs for the period of February 1993 were carried out for the North Sea area using the coarse grid implementation with stereographical projection (see Section 3.2.2). Two runs labelled C3 and C4 were retained. Except for the propagation scheme, the runs are identical. It was found that in general, the model produces higher significant wave height when using the octant coordinate than when using the quadrant system. Fig. 8 illustrates the significant wave height differences between run C4 (octant propagation scheme) and run C3 (quadrant propagation scheme) on February 21, 1993 at 0000 GMT. At that moment, waves in the central North Sea were quite high (~ 8 m significant wave height). In the central part, differences up to about 15 cm can be observed. However, more importantly close to some coasts, e.g., along the coast of eastern Scotland and along the coast to the southeast of Orkney and the Shetlands, differences can be higher than 30 cm. This will have consequences on boundary conditions generated for more detailed assessment of the wave conditions in these areas.

3.3.1.4. Currents. To take into account the non-stationary current field and water level changes, the WAMC4-P was prepared for coupling with a storm/surge model in a two-way system. The model can accept hydrodynamic fields (currents and water level) from and return wave-related information (radiation and surface stresses) to the hydrodynamic model. Ozer et al. (2000) explore the interaction mechanisms and their importance.

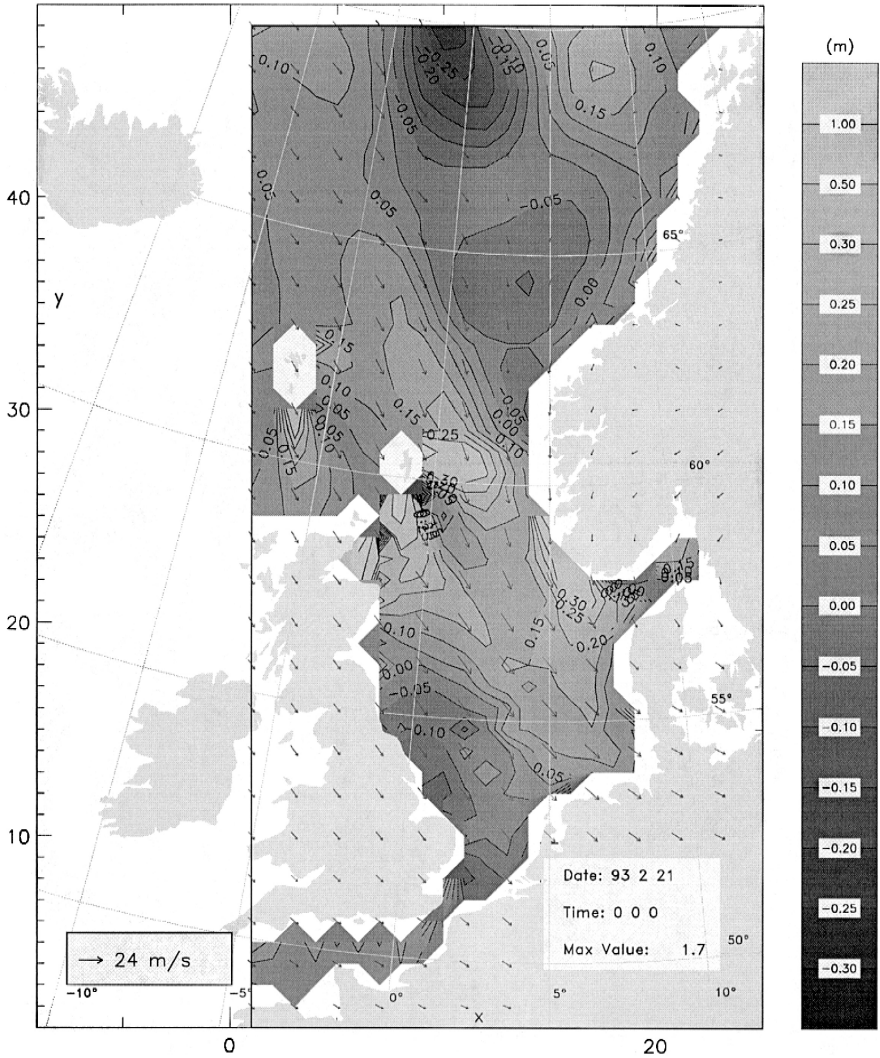


Fig. 8. The significant wave height difference between the run with the octant (C4) and the quadrant (C3) propagation scheme at 0000 GMT February 21, 1993 (C4 minus C3).

3.3.2. Source terms

3.3.2.1. Numerical limiters. In the standard WAMC4, the source term equation (Eq. 1 without the advection terms) is solved by the following finite difference approximation:

$$\frac{F_{i,j,k,l}^{n+1} - F_{i,j,k,l}^n}{\Delta t} = (1 - \alpha)S_{i,j,k,l}^n + \alpha S_{i,j,k,l}^{n+1}, \tag{8}$$

where i and j denote the position in geographical space, k and l represent the position in the wave direction and relative frequency space and α is in the range $[0,1]$.

Since the source functions depend non-linearly on the spectrum F , Taylor expansions were introduced. By disregarding the negligible off-diagonal contribution of the function derivatives [(Komen et al., 1994)] in the Taylor expansions, the increments in spectral energy density due to the source terms for one time step may be expressed as:

$$\Delta_{\text{int}} F_{i,j,k,l}^n = \Delta t S_{i,j,k,l}^n \left[1 - \Delta t \alpha \Lambda_{i,j,k,l}^n \right]^{-1}, \tag{9}$$

where $\Lambda_{i,j,k,l}^n$ is the diagonal matrix of the partial derivatives of the source function. A forward time splitting technique is used ($\alpha = 1$) except for positive $\Lambda_{i,j,k,l}^n$ when because of the obvious numerical instability, an explicit technique is used ($\alpha = 0$). However, the explicit implementation is not generally stable [(Press et al., 1994)], so a limiter on the increments in wave energy was imposed. It is expressed as:

$$\Delta_{\text{int}} F_{\text{max}}^n = 6.2 \times 10^{-5} f^{-5} \Delta t / 1200. \tag{10}$$

Hersbach and Janssen (1999) found that for applications with a very small spatial grid such as in coastal regions, the old limiter (Eq. 10) was so severe that the growth curves did not scale properly with the air friction velocity. They revised the limiter (further referred to as the HJ limiter) to solve the above problem:

$$\Delta_{\text{int}} F_{\text{max}}^n = 3 \times 10^{-7} g \tilde{u}_a^* f_c f^{-4} \Delta t, \tag{11}$$

where f_c is the cut-off frequency, Δt is the source term integration time step and \tilde{u}_a^* is determined by:

$$\tilde{u}_a^* = \max(u_a^*, g f_{\text{PM}}^* / f); \quad f_{\text{PM}}^* = 5.6 \times 10^{-3}, \tag{12}$$

with u_a^* the air friction velocity and f_{PM}^* the dimensionless Pierson–Moskowitz peak frequency. Hersbach and Janssen (1999) show that the limiter in Eq. 11 is scale-invariant because it can be written just in terms of non-dimensional quantities. It was released as a patch to WAMC4 [(Hasselmann, 1996)]. According to Luo and Sclavo (1997), the HJ limiter may give rise to problems for low frequencies in relatively calm conditions since the value for \tilde{u}_a^* will be much larger in low frequencies than in the high frequencies. They use the mean frequency f_m instead of the cut-off frequency f_c (note that Hersbach and Janssen, 1999 also mention this possibility):

$$\Delta_{\text{int}} F_{\text{max}}^n = 3 \times 10^{-7} g \tilde{u}_a^* f_m f^{-4} \Delta t, \tag{13}$$

where

$$\tilde{u}_a^* = \max(u_a^*, g f_{\text{PM}}^* / f). \tag{14}$$

However, when a small enough time step is used, WAM is numerically stable for fetch-limited growth cases even when no limiter is used. This demonstrates that the problem arises from the numerical integration scheme rather than the underlying physical equations for wave growth. The imposition of a limiter prevents convergence to the continuum solution as the time increment is decreased and so Hargreaves and Annan (1999) argue that a better approach would be to dispense with the limiter and improve the integration scheme. By constraining $\Lambda_{i,j,k,l}^n$ to always be negative, the forward time

scheme ($\alpha = 1$) can always be used and this gives greatly improved results over the standard method (this method is referred to, hereafter, as the HA method). However, stability cannot be absolutely guaranteed for any computationally reasonable time step, since the integration of source terms is a ‘stiff’ problem [(Press et al., 1994)]. The method is found to be stable for fetch-limited growth test cases up to high wind speeds as illustrated below, but when the model is run with the HA limiter in real applications, it is found that instabilities do sometimes occur. The model has been found to be well behaved in real applications when the HJ limiter is imposed on the highest frequencies (> 0.25 Hz) while employing the HA method. The HA method will be included as an option in the disseminated WAMC4-P code.

To illustrate the effect of limiters, the Holderness set-up is again used with a uniform southerly wind of 30 m s^{-1} to drive the model. When the limiter is completely removed from the WAMC4 coding with the standard integration scheme, the model is stable only for very small time steps. Therefore, reference runs were made running with a 10-s source term time step. Fig. 9 shows the fetch-limited growth curves for model runs using the HA method and the HJ limiter, and the reference run for comparison. For a time step of 300 s, the HJ limiter and the HA method produce similar results. However, as the time step is decreased, the HA method converges to the reference run whereas the HJ limiter run does not.

Fig. 10 shows a further comparison of the results. This figure shows the fetch-limited growth wave spectra obtained for fetches equivalent to the Holderness wave buoys (see Prandle et al., 2000). The effect of the HA method only seems critical in high growth situations, and it only has a significant effect in small fetch situations near coasts, consistent with the remarks in Section 3.3.1.2, that correct representation of rapid variations demands small time steps. As can be seen from Fig. 10, all three runs produce almost identical results at fetches of 100 km.

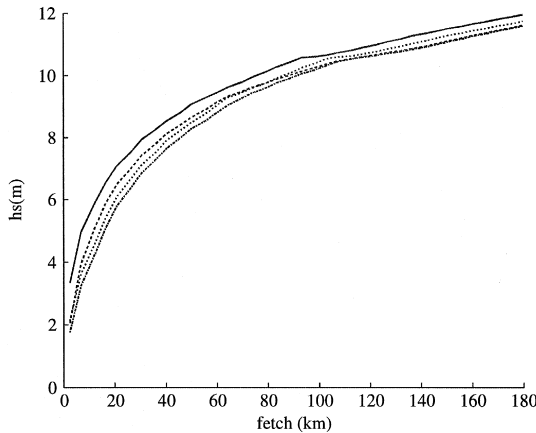


Fig. 9. Fetch-limited growth curves. The solid line shows the reference run, the dotted line the run with a 10 s time step and Hersbach limiter, the dot-dashed line the run with a 200-s time step and Hersbach limiter and the dashed line shows the 300-s run with the Hargreaves–Annan method. This last method is indistinguishable from the reference run for a 10-s time step.

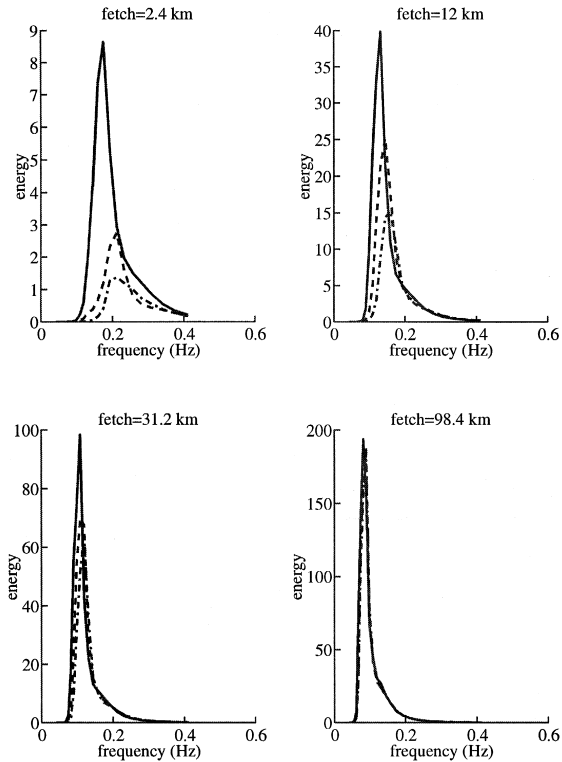


Fig. 10. Wave spectra at different fetches. The solid lines are the reference run with 10 s time step, the dot-dashed and dashed lines are for the Hersbach limiter and Hargreaves–Annan approach, respectively, both with a 300-s time step.

3.3.3. Bottom friction and depth-induced breaking

Four additional bottom friction formulations for pure wave conditions have been implemented in WAMC4-P. They are the formulations of Hasselmann and Collins (1968), Collins (1972), Madsen et al. (1988) and Weber (1991). A detailed discussion on these formulations as well as on the empirical JONSWAP formulation, which is implemented in the standard WAMC4, can be found in Luo and Monbaliu (1994). An illustration of their use in a practical situation can be found in Luo et al. (1996).

Bottom friction formulations accounting for a combined wave–current field have been introduced as well. Several theoretical models for the bottom friction in combined wave–current flows have been developed and have advanced our knowledge of wave–current interactions (e.g., [Grant and Madsen, 1979; Christoffersen and Jonsson, 1985]). However, these models were derived for a wave motion corresponding to a single period wave. Only recently has Madsen (1994) derived a model for turbulent wave–current bottom boundary layer flows with wave motion described by its directional spectrum. The formulations of Christoffersen and Jonsson (1985) and Madsen (1994) have been implemented in WAMC4-P, but they have not yet been fully tested. An interesting

discussion on wave–current interaction observations in the Holderness area is given by Wolf and Prandle (1999) and Wolf (1999).

To simulate depth-induced wave breaking, a source term based on the theory of Battjes and Janssen (1978) has been added in WAMC4-P. In this theory, it is assumed that depth-induced wave breaking does not affect the shape of the spectrum itself, which has been experimentally verified by Beji and Battjes (1993). For the mathematical expression of the source term and for a practical illustration, the reader is referred to van Vledder et al. (1995) and Luo (1995). Since depth-induced wave breaking is a dominant source term in shallow water applications, a more detailed analysis of breaking formulations should be carried out. An interesting study on the introduction of other model formulations has been executed by Becq and Benoit (1996). They have compared the behaviour of four different formulations.

3.4. I/O and some other peculiarities

Boundary conditions are now interpolated in time within the WAMC4-P model. When the standard WAMC4 was run in a nested mode, the boundary conditions for a finer grid are written to the computer disk at every coarse grid propagation time step. Those boundary conditions needed to be interpolated in space and time for the finer grid (the time–space resolution depends on the characteristics of the finer grid), and stored for the whole period on the computer disk. For high-resolution applications, this meant that nested grid runs demanded very high disk storage capacity. In order to avoid these disk storage problems, two changes were made to the code. Firstly, the interpolation of the boundary conditions in time and space is now executed in the nested grid, drastically reducing the disc space needed and the computing time. This was done by incorporating the stand-alone boundary interpolation routine into the new WAMC4-P code. Secondly, the user can now define the time step to write boundary conditions for a finer grid application. The statistical parameters of the spectrum do not change much in the time span of a few minutes. In order to compare the differences in disk usage and results (wave heights) between the original WAMC4 and the two disk usage optimisations implemented, the three-level nested grid system in spherical coordinates described in Section 3.2.2 was used. For this test, three runs were carried out. The first run used the standard WAMC4 procedure. This means that the boundary conditions were saved in every propagation time step for the coarse and intermediate grids. These boundary conditions then need to be interpolated in time (every propagation time step in the nested grid) and space, and all the interpolated information need to be stored on disk. In the second run, the boundary conditions were interpolated in the nested runs themselves (intermediate and fine grids). In the third run, not only was the interpolation of boundary conditions in time and space done inside the nested runs (as in the second run), also the output time step for the boundary conditions from the coarse and intermediate grid was user-defined. The wave model was run with an output time step for the boundary conditions of 40 min for the coarse and 20 min for the intermediate grid. Note that the propagation time step was 20 min for the coarse and 4 min for the intermediate grid. The savings in disk storage space are enormous (see Fig. 11). The output of the model is

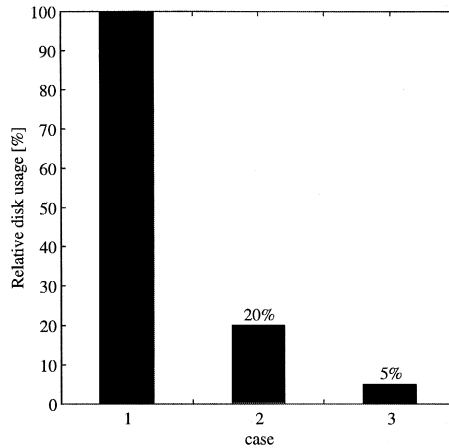


Fig. 11. Relative disk usage for different optimisations in output boundary conditions.

almost identical (not shown). This is of considerable practical importance for operational modelling.

Some additional details were changed in the code. The constraint in the original scheme of WAMC4, which limits all time steps to be a multiple of 1 min, has been removed. All the dates are now represented by a 12-digit character number (with the format *yymmddhhmmss*, where *yy* indicates the year, *mm* is for month, *dd* for day, *hh* for hour, *mm* for minute and *ss* for second). Therefore, all model time steps (wind I/O time steps, source term integration time step, propagation time step and all output time steps) can be specified as integer in seconds or hours (if greater than 1 h). They do not have to be in multiples of 1 min as limited by the original scheme of WAMC4.

To avoid problems with fractional numbers, the dimension and location of the computational grid must now be given in seconds. To solve rounding problems when comparing the location of grid points, these are now defined with accuracy better than 1 s.

In a small area covered by a high-resolution grid nested into a coarse grid, a steady state situation can be reached before boundary conditions are changed. In this case, the model will continue integrating in time unnecessarily. An option has been installed in the code so that consecutive wave fields are compared and a warning message is printed if a steady state is found. The second moment period (T_{m02}) is quite often recorded by buoys. In order to compare the model data to these measurement data, a subroutine to compute that parameter was added in the WAMC4-P model code. Also the calculation of the radiation stresses is now included. This is of interest when the wave model is coupled to a hydrodynamic model (see Ozer et al., 2000 for more details).

3.5. Further work

Non-linear interactions in shallow water, the so-called triads, are not yet accounted for in the model. Young and Eldeberky (1998) have seen some evidence of triad

interactions at fairly high values of the relative depth ($k_p d$, where k_p is the wave number at the spectral peak and d is the water depth) when analysing data from experiments in a shallow lake. They suggest that the effects of such interactions might not be significant only in the shoaling region, but also may need to be introduced in transitional water depths found on many continental shelves.

Although several formulations for bottom friction energy dissipation have been coded, which one to use in operational applications is far from clear.

Little or no effort has been made up to now to assimilate data (wave, wind, bathymetry, etc.) in high-resolution wave model applications. For coastal applications, the data needs are very demanding, since the details of the directional energy distribution are very important. Moreover, memory in the system is short-lived. Waves entering the system at the seaward boundary arrive at the coast in a period of a few hours and dissipate most, if not all, of their energy.

4. Summary and conclusions

New features have been added, and several changes to the standard WAMC4 model code were necessary in order to run it efficiently in shallow water applications. The restriction of having a source term integration time step smaller than or equal to the propagation time step was relaxed. This change enabled the source term integration time step to be much longer than the propagation time step and, therefore, the CPU time for high-resolution applications could be reduced considerably. Additional reduction of the CPU time was obtained by the introduction of a split-frequency time step.

Besides the changes to speed up the computation, the propagation coordinates system can be optionally chosen to be octant or quadrant. The role of the limiter in the source term integration was discussed. Different bottom friction formulations and the Battjes–Janssen expression for the energy dissipation due to depth-induced wave breaking were added to the WAM code in the hope of obtaining a more reliable evaluation of the energy decay in shallow water areas.

The procedure of making nested runs was changed in order to save disk space. As a side-benefit, time spent on I/O was also decreased. Other minor changes were made to enhance the model performance in high-resolution applications, and the option to output additional wave parameters was included.

As a result of all these changes, applications of the WAMC4-P model code in shallow water areas, where high-spatial resolution is needed, has become feasible and economical. Together with all the other works carried out within the PROMISE project to deal with the interaction of the wave field with the current field [(Ozer et al., 2000)], the WAMC4-P code provides a powerful tool to further explore the modelling of wave spectra in coastal regions. As such, it forms an important part of a pre-operational framework of mathematical modelling tools necessary to quantify sediment transport in the coastal and nearshore zone. It is hoped that the improved description of the wave field and of the hydrodynamic field will lead to more sophisticated parameterisation of the hydrodynamic forces in sediment transport modelling.

Acknowledgements

This study was partially carried out with financial support from the EU MAST III Programme, contract MAS3-CT9500025. Several parts of the WAM code enhancements described above have been, at one time or another, added to the code because of specific needs at a particular institute. The PROMISE group tried to bring many of these different items together in one code, and hereby wish to thank the many anonymous contributors. The original WAMC4 code was obtained from the Max-Planck Institut für Meteorologie.

References

- Battjes, J.A., Janssen, J.P.F.M., 1978. Energy loss and set-up due to breaking of random waves. Proc. 16th Int. Conf. Coastal Eng., 569–587.
- Battjes, J.A., 1994. Shallow water wave modelling. Proc. Int. Symp. Waves — Phys. Numer. Modell., University of British Columbia, Vancouver I, 1–23.
- Becq, F., Benoit, M., 1996. Implémentation et comparaison de différents modèles de houle dans la zone de déferlement. EDF, Report HE-42/96/037/A, in French.
- Beji, S., Battjes, J.A., 1993. Experimental investigation of wave propagation over a bar. Coastal Eng. 19, 151–162.
- Booij, N., Ris, R.C., Holthuijsen, L.H., 1999. A third-generation wave model for coastal regions: 1. Model description and validation. J. Geophys. Res. 104 (C4), 7649–7666.
- Cavaleri, L., Sclavo, M., 1998. Characteristics of the quadrant and octant advection schemes in wave models. Coastal Eng. 34, 221–242.
- Collins, J.I., 1972. Prediction of shallow water spectra. J. Geophys. Res. 93 (C1), 491–508.
- Christoffersen, J.B., Jonsson, I.G., 1985. Bed friction and dissipation in a combined current and wave motion. Ocean Eng. 12, 387–423.
- Grant, W.D., Madsen, O.S., 1979. Combined wave and current interaction with a rough bottom. J. Geophys. Res. 84, 1797–1808.
- Günther, H., Hasselmann, S., Janssen, P.A.E.M., 1992. The WAM model Cycle 4. Report No. 4, Hamburg.
- Günther, H., Rosenthal, W., 1997. Shallow water wave modelling with non-linear dissipation. Dtsch. Hydrogr. Z. 49, 431–444.
- Hargreaves, J.C., Annan, J.D., 1999. Integration of source terms in a third-generation wave model. J. Phys. Oceanogr., Submitted.
- Hersbach, H., Janssen, P., 1999. Improvements of the short fetch behaviour in the WAM model. J. Atmos. Oceanic Technol. 16, 884–892.
- Hasselmann, K., Collins, J.I., 1968. Spectral dissipation of finite-depth gravity waves due to turbulent bottom friction. J. Mar. Res. 26, 1–12.
- Hasselmann, S., 1996. Personal communication.
- Komen, G.J., Cavaleri, L., Donelan, M., Hasselmann, K., Hasselmann, S., Janssen, P.A.E.M., 1994. Dynamics and Modelling of Ocean Waves. Cambridge Univ. Press, Cambridge.
- Luo, W., Monbaliu, J., 1994. Effects of the bottom dissipation formulation on the energy balance for gravity waves in shallow water. J. Geophys. Res. 99 (C9), 18501–18511.
- Luo, W., 1995. Wave modelling in shallow water. PhD Thesis, Civil Engineering Department, Katholieke Universiteit Leuven, Belgium.
- Luo, W., Monbaliu, J., Berlamont, J., 1996. Bottom friction dissipation in the Belgian coastal waters. Proc. 25th Int. Conf. Coastal Eng., 836–849.
- Luo, W., Sclavo, M., 1997. Improvement of the third-generation WAM Model (Cycle 4) for applications in the nearshore regions. Proudman Oceanographic Laboratory, Internal Document No. 116.

- Madsen, O.S., Poon, Y.K., Graber, H.C., 1988. Spectral wave attenuation by bottom friction: theory. Proc. 21st Conf. Coastal Eng., 492–504.
- Madsen, O.S., 1994. Spectral wave–current bottom boundary layer flows. Proc. 24th Conf. Coastal Eng., 384–398.
- Monbaliu, J., Zhang, M.Y., de Backer, K., Hargreaves, J., Luo, W., Flather, R., Carretero, J.C., Gomez Lahoz, M., Lozano, I., Stawartz, M., Günther, H., Rosenthal, W., Ozer, J., 1997. WAM model intercomparisons — North Sea. Proudman Oceanographic Laboratory, Report No. 47.
- Monbaliu, J., Hargreaves, J.C., Carretero, J.C., Gerritsen, H., Flather, R., 1999. Wave modelling in the PROMISE project. Coastal Eng. 37, 379–407.
- Monbaliu, J., Padilla, R., Osuna, P., Hargreaves, J., Flather, R., Carretero, J.C., 1998. Shallow water version WAM-C4-S.01 documentation. Proudman Oceanographic Laboratory, Report No. 52.
- Ozer, J., Padilla-Hernández, R., Monbaliu, J., Alvarez Fanjul, E., Carretero Albiach, J.C., Osuna, P., Yu, J.C.S., Wolf, J., 2000. A coupling module for tides, surges and waves. This volume.
- Prandle, D., 2000. Operational oceanography in coastal waters. This volume.
- Prandle, D., Hargreaves, J.C., McManus, J.P., Campbell, A.R., Duwe, K., Lane, A., Mahnke, P., Shimwell, S., Wolf, J., 2000. Tide, wave and suspended sediment modelling on an open coast — Holderness. This volume.
- Press, W.H., Teukolsky, S.A., Vetterling, W.T., Flannery, B.P., 1994. Numerical Recipes in FORTRAN: The Art of Scientific Computing. Cambridge Univ. Press.
- Ris, R.C., 1997. Spectral modelling of wind waves in coastal areas. PhD Thesis, Delft University of Technology, the Netherlands.
- Ris, R.C., Holthuijsen, L.H., Booij, N., 1999. A third-generation wave model for coastal regions: 2. Verification. J. Geophys. Res. 104 (C4), 7667–7681.
- Schneggenburger, C., 1998. Spectral wave modelling with non-linear dissipation. PhD Thesis, University of Hamburg, GKSS External Report 98/E/42.
- Schneggenburger, C., Günther, H., Rosenthal, W., 2000. Spectral wave modelling with non-linear dissipation: validation and applications in a coastal tidal environment. This volume.
- van Vledder, G.Ph., de Ronde, J.G., Stive, M.J.F., 1995. Performance of a spectral wind-wave model in shallow water. Proc. 24th Int. Conf. Coastal Eng., 761–774.
- Weber, S.L., 1991. Eddy viscosity and drag law models for random ocean wave dissipation. J. Fluid Mech. 232, 73–98.
- Wolf, J., Prandle, D., 1999. Some observations of wave–current interaction. Coastal Eng. 37, 471–485.
- Wolf, J., 1999. The estimation of shear stresses from near-bed turbulent velocities for combined wave–current flows. Coastal Eng. 37, 529–543.
- Young, I.R., Eldeberky, Y., 1998. Observations of triad coupling of finite depth wind waves. Coastal Eng. 33, 137–154.